Pergamon

Int. J. Multiphase Flow Vol. 23, No. 6, pp. 1007–1029, 1997

Printed in Great Britain
PII: S0301-9322(97)00034-7
0301-9322/97 $17.00 + 0.00

PRESSURE MEASUREMENTS AND CONVECTION VELOCITY EVALUATIONS IN TWO-PHASE FLOW

A. L. SAMWAYS†, L. J. S. BRADBURY‡ and H. H. BRUUN
Department of Mechanical and Manufacturing Engineering, Bradford University, Bradford BD7 1DP, U.K.

(Received 15 October 1996; in revised form 24 April 1997)

Abstract—This paper describes an experimental and theoretical study of convected pressure fields in air/water two-phase flows. An air/water pipe flow loop was designed with a vertical test section. A detailed experimental evaluation was carried out on the use of differential pressure transducers for wall pressure measurements. It was established both experimentally and theoretically that the dispersed (bubble) phase will only create very low fluctuating hydrodynamic pressures, resulting in major vibrations and instrumentation problems. Detailed laborious transducer designs and tests eliminated these problems, resulting in an accurate differential pressure technique for the study of convected pressure fields related to the bubble motion.

Theoretical pressure predictions and auto- and cross-correlation measurements have demonstrated that the measured convected pressure field is caused by slow moving bubbles travelling in the 'entrapment' boundary layer next to the wall, rather than being a measure of the area averaged bubble velocity.

Key Words: pressure fluctuations, two-phase flow, differential pressure transducer, convected pressure field

1. INTRODUCTION

Very few attempts have been made to investigate pressure fluctuations in two-phase flows. Comparison of statistical data from the fluctuating wall static pressure and visual observations have been used in a number of investigations for flow regime identification related to bubbly, spherical-cap bubbles, slug, froth, annular and mist flow in vertical pipes. Techniques were developed using both a single pressure transducer and two or more transducers separated in the longitudinal direction of the mean flow.

In one of the earliest investigations, by Nishikawa *et al.* (1969), a detailed study was carried out using five static strain gauge transducers connected to tappings at 0.1, 0.25, 0.5 and 1 m intervals from the first tapping in a transparent 26 mm smooth bore pipe. Flow regime identification was attempted based on the shape of the probability density function (pdf) distribution and the values of the standard deviation and the characteristic length scale of the auto-correlation. In the bubbly and annular flow regimes, the shape of the pdf distribution roughly equated to a normal Gaussian distribution, while in most cases of slug and froth flows the pdf exhibited twin peaks. No conclusive flow regime identification method was developed.

Further pressure measurement investigations have been reported by Tutu (1982) for an air/water flow loop having a 2.5 m long test section with an internal diameter D of 52.2 mm, using two Endevco model 8506-5 piezoresistive pressure transducers, separated axially by $D/2$ and flush mounted with the inside pipe wall along the same vertical axis. Matsui (1984) studied a nitrogen gas/water flow in a pipe with an internal diameter D of 22 mm, using four static piezoresistive pressure transducers placed in pairs with an axial separation of $D/2$. Each pair of transducers was separated axially by 200 mm, and mounted as near flush as possible with the internal diameter of the transparent pipe. Differential pressure signals were obtained digitally for

†Formerly at the University of Plymouth, present address: The Glacier Metal Co. Ltd., Wintermay Lane, Ilminster, Somerset TA19 9PH, U.K.
‡Formerly at the University of Plymouth.

both the transducer pairs (separation $D/2 = 11$ mm) and between transducers in the two pairs (separation 200 mm).

Tutu (1982), like Nishikawa *et al.* (1969), also made static pressure measurements P_2 and P_1 from upstream and downstream pressure transducers. However, unlike Nishikawa *et al.* (1969), the two static pressure signals were also subtracted using an analogue difference circuit to obtain the differential pressure $\Delta P = P_1 - P_2$ which was also recorded and analysed. Tutu evaluated and plotted the pdf, skewness and flatness factors for ΔP, and claimed that a discrimination technique for the various flow regimes could be based on the magnitude of the skewness and flatness factors from a single differential pressure signal ΔP. In bubbly, vertically upward air/water two-phase flow, he observed that the pdf exhibits a single peak centred approximately around the position of the area averaged gas void fraction $\langle \epsilon \rangle$. A similar observation was made by Matsui (1984), who also claimed that flow regimes could be identified using the differential signal based on the long separation length.

Matsui (1984) also cross-correlated two differential pressures ΔP_a and ΔP_b for the spherical-cap bubble flow regime. The position of the temporal delay peak in the cross-correlation was assumed to correspond to the time of flight of the dispersed phase and the corresponding gas rise velocity was evaluated as 0.37 m/s. This compares well with the average rise velocity measured from serial photographs of 0.36 m/s. Within the bubbly two-phase flow, convected disturbances will be primarily generated by the passage of the dispersed bubbly phase through the continuous phase. Therefore it follows that the convected disturbance velocity of the naturally occurring pressure fluctuations evaluated by correlation techniques may reflect the velocity of the dispersed phase. However, Matsui (1984) could obtain no cross-correlation for the bubbly flow regime. One reason for this may be due to the large transducer separation distance of 200 mm.

The detailed theoretical and experimental work presented in this paper demonstrates that the differential wall pressure signal is dominated by the convected pressure field from slow moving bubbles travelling in the wall boundary layer. This paper presents a description of these findings.

2. SOURCES OF PRESSURE FLUCTUATIONS IN BUBBLY VERTICAL TWO-PHASE FLOW

The pressure at any point in a two-phase flow is caused either by the direct hydrodynamic nature of the two-phase flow itself, or by unwanted pressure pulsations from pumps, restrictions/intrusions to the flow or vibrations acting upon the flow loop from external sources. This section will (a) discuss the hydrodynamic pressure effects, (b) describe how differential pressure measurements can be used to minimize the extraneous vibration effects, and it will also be demonstrated in section 4 by comparison of theory and experiments that the differential pressure from wall tappings can be used to record the convected unsteady pressure field from nearby bubbles.

In the theoretical analysis of the pressure field around bubbles (section 2.1), they will be treated as solid spheres, and to determine the validity of this assumption, comparisons are made between experiments involving bubbles, solid spheres and theory. Also, as discussed by Peebles and Garber (1953), a near-spherical air bubble in a continuous water phase tends to act like a solid sphere due to the collection of contaminates at the interface. It was observed in our study that the bubbles were ellipsoidal in shape, but it is not unreasonable to treat a discrete bubble as a solid sphere of diameter d in order to estimate the amplitude of the pressure fluctuation caused by a bubble's motion.

Naturally occurring pressure fluctuations in a bubbly two-phase flow are caused by a combination of many effects. The main contributors as discussed in the following sections are:

(i) pressure fluctuations caused by variations in the continuous phase velocity profile around a near-spherical bubble;
(ii) pressure fluctuations in the continuous phase caused by the continuous phase background turbulence and the wake generated by a bubble.

2.1. *Pressure fluctuations caused by variations in the continuous phase velocity profile around a near-spherical bubble*

To estimate the amplitude of pressure waves created by a bubble' s motion as it disturbs the continuous phase it is flowing through, consider initially the problem where the continuous phase is stagnant and bubbles rise through the continuous phase with a constant velocity V_∞.

Using this comparison, Butler's (1953) sphere theorem, as discussed in e.g. Milne-Thomson (1960) for a stationary sphere in an infinite fluid having a uniform velocity, can be translated to describe a sphere travelling at a constant velocity through a stationary fluid. Using Butler's sphere theorem in this form, the pressure field surrounding a moving bubble can be calculated and hence the amplitude of the pressure fluctuation caused by a bubble's motion can be estimated.

Consider the motion of a solid sphere of radius a, travelling at a velocity V_∞, in a stationary infinitely large incompressible inviscid fluid, as shown in figure 1. If we assume the flow of the fluid displaced by the sphere to be both axisymmetric and irrotational about the axis of the sphere's motion, then Butler's sphere theorem gives the velocity potential Φ for this case as

$$\Phi = V_\infty\left[r + \frac{a^3}{2r^2}\right]\cos\theta \qquad [1]$$

where θ is the angle between the axis of bubble motion, in the direction of bubble motion, and a point n in the infinite fluid at a distance r from the centre of the sphere.

Using spherical polar coordinates, the r and θ velocity components are given by

$$V_r = -\frac{\partial\Phi}{\partial r} = -V_\infty\left[1 - \frac{a^3}{r^3}\right]\cos\theta \qquad [2]$$

$$V_\theta = -\frac{1}{r}\frac{\partial\Phi}{\partial\theta} = -\frac{V_\infty}{r}\left[r + \frac{a^3}{2r^2}\right]\sin\theta \qquad [3]$$

and if we assume the velocity field surrounding the sphere to be symmetrical about the axis of motion

$$V_\Psi = -\frac{1}{\sin\theta}\frac{\partial\Phi}{\partial\Psi} = 0 \qquad [4]$$

The magnitude of the velocity vector is defined by

$$\underline{V}^2 = V_r^2 + V_\theta^2 + V_\Psi^2 \qquad [5]$$

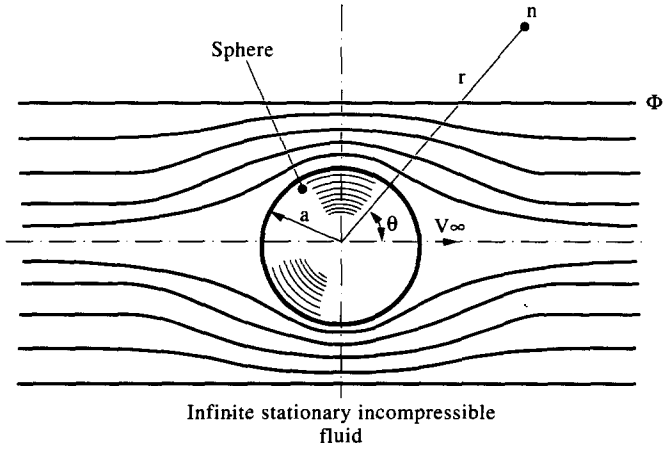

Figure 1. Notation for Butler's sphere theorem for a sphere travelling with a constant velocity through an infinitely large incompressible inviscid fluid.

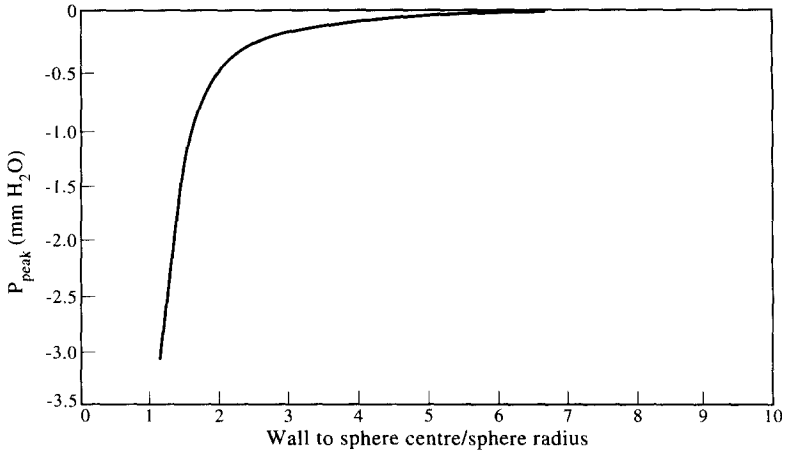

Figure 2. Theoretical peak pressure fluctuations P_{peak} caused by the motion of a single sphere as a function of pipe wall-to-sphere centre separation distance, $V_\infty = 0.25$ m/s. sphere radius $a = 3$ mm.

and so

$$\underline{V}^2 = V_\infty^2\left[1 + \frac{a^3}{r^3}[1 - 3\cos^2\theta] + \frac{a^6}{4r^6}[1 + 3\cos^2\theta]\right] \quad [6]$$

The pressure P and the magnitude of the velocity $\underline{V}$ at any point can be related to the pressure at infinity (where $V = 0$) by Bernoulli's equation

$$P = P_0 - \frac{1}{2}\rho_l \underline{V}^2 \quad [7]$$

where P_0 is the pressure at infinity. Therefore

$$P = P_0 - \frac{1}{2}\rho_l V_\infty^2\left[1 + \frac{a^3}{r^3}[1 - 3\cos^2\theta] + \frac{a^6}{4r^6}[1 + 3\cos^2\theta]\right] \quad [8]$$

The velocity potential between any point on the sphere's surface and any point in the infinite fluid can be shown to be a maximum on a plane perpendicular to the axis of bubble motion ($\theta = 90°$) passing through the centre of the sphere. Therefore, by setting $\theta = 90°$ in [8], we obtain a solution for the peak pressure P_{peak} seen by any fixed point in the infinite fluid on a plane perpendicular to the axis of flow at a distance r from the centre of the sphere.

$$P_{peak} = (P - P_0) = -\frac{1}{2}\rho_l V_\infty^2\left[\left[1 + \frac{a^3}{2R^3}\right]^2 - 1\right] \quad [9]$$

where R is the perpendicular distance, with respect to the sphere trajectory, from the centre of the sphere to the fixed measuring point.

Apply this theory to a typical practical case of a sphere of radius $a = 3$ mm, travelling at a constant velocity $V_\infty = 0.25$ m/s in water ($\rho_l = 1000$ kg/m^3). The corresponding figure 2 shows how the magnitude of the peak pressure P_{peak} (evaluated in mm H_2O) due to this effect will vary as a function of the perpendicular distance R from the centre of the sphere's trajectory to the measuring point in an infinite fluid. The figure clearly shows that the magnitude of the peak pressure caused by a bubble's motion will diminish rapidly with increasing bubble-to-measuring point perpendicular separation distance, with P_{peak} being 2 mm H_2O at $1.5a$ and only 0.05 mm H_2O at a distance of $4a$.

To extract information about the convected flow field, a correlation technique may be used with two fixed points, 1 and 2, separated by a distance l in the axial direction. For the two points, 1 and 2, in the fluid, the theoretical differential pressure ΔP between these two points caused by

the bubble's motion is given by

$$\Delta P = P_1 - P_2 \qquad [10]$$

In the following analysis, it will be assumed that the sphere is travelling at a constant velocity V_∞ along a fixed trajectory which is at a constant perpendicular distance R from the two points 1 and 2, and 1 and 2 are separated by a distance l which is parallel to the trajectory of the sphere. Using the notation shown in figure 3 and substituting [8] into [10] for the pressures P_1 and P_2, we obtain

$$\Delta P = \frac{1}{2}\rho_l V_\infty^2 \left\{ \left[1 + \frac{a^3}{r_2^3}[1 - 3\cos^2\theta_2] + \frac{a^6}{4r_2^6}[1 + 3\cos^2\theta_2] \right] - \left[1 + \frac{a^3}{r_1^3}[1 - 3\cos^2\theta_1] + \frac{a^6}{4r_1^6}[1 + 3\cos^2\theta_1] \right] \right\} \qquad [11]$$

where

$$r_1 = R/\sin\theta_1 \quad \text{and} \quad r_2 = ((r_1\cos\theta_1 + l)^2 + R^2)^{1/2} \qquad [12]$$

and the angles θ_1 and θ_2 are the angles between the points 1 and 2 and the centre of the sphere along its trajectory respectively.

It is instructive to look at the calculated pressures $P_1(t)$ and $P_2(t)$ and the differential pressure $\Delta P(t) = P_1(t) - P_2(t)$ as a sphere travels past the pressure tappings 1 and 2, which will be assumed to be wall tappings. It should be noted at this time that [9] is for a sphere travelling through an infinite fluid and therefore does not allow for the effect of a pipe wall. However, as [11] is a differential equation involving two points with the same distance from the bubble to the wall, this effect should be eliminated to first order.

The calculated temporal variation in $\Delta P(t)$ [11] is illustrated in figure 4 for a sphere of radius $a = 3$ mm travelling past point 1 and 2 with a perpendicular distance $R = 4.5$ mm. The time $t = 0$ corresponds to the sphere being directly opposite tapping number 1. The normalised pressures $P_1(t)/\frac{1}{2}\rho_l V_\infty^2$, $P_2(t)/\frac{1}{2}\rho_l V_\infty^2$ and $(P_1(t) - P_2(t))/\frac{1}{2}\rho_l V_\infty^2$ are shown in curves a, b and c of figure 4 respectively.

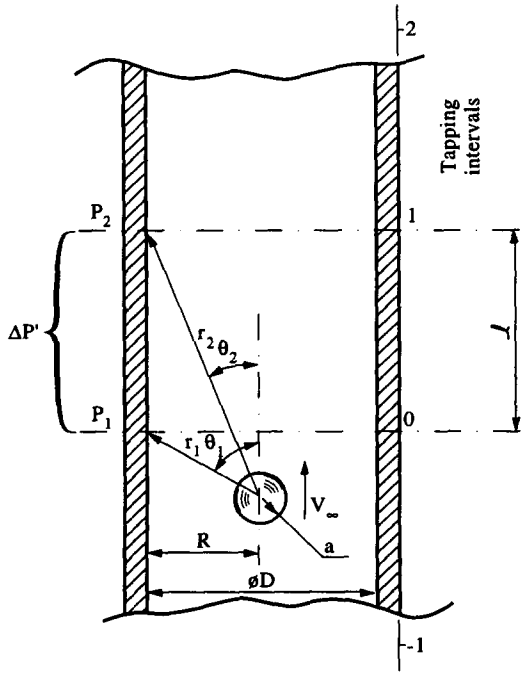

Figure 3. Geometry and notation for differential pressure measurements.

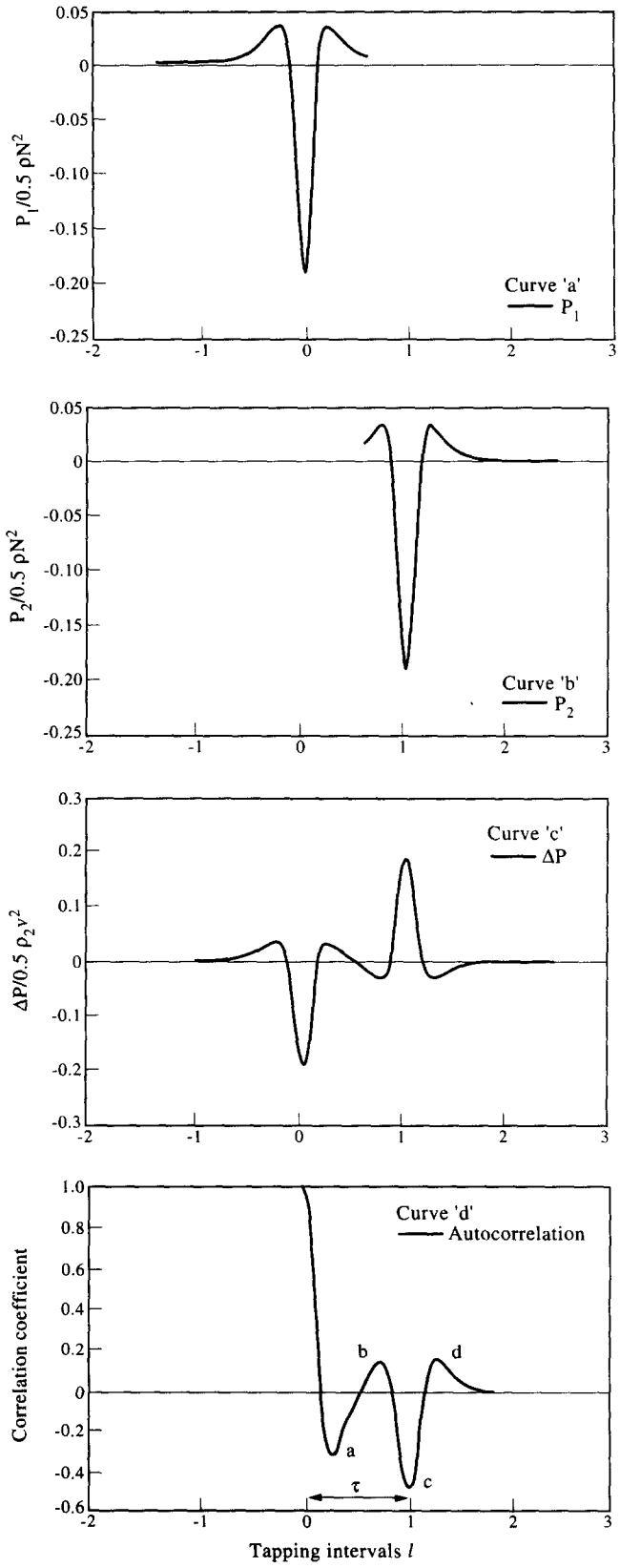

Figure 4. Calculated pressure signals generated as a sphere of radius $a = 3$ mm travels with a constant velocity V_∞, past two fixed pressure measuring points, 1 and 2, at a distance $R = 4.5$ mm.

It can clearly be seen from figure 4(c) that the pressure wave created by a moving sphere observed by the differential pressure $\Delta P = P_1 - P_2$ is an inversely symmetrical curve about a point midway between the measuring points 1 and 2, at $l/2$, or 0.5 tapping intervals. It is also observed from figure 4(c) that the maximum amplitude of the pressure wave occurs when one of the two fixed measurement points, 1 or 2, is perpendicularly opposite the centre of the sphere with respect to the sphere's trajectory. The existence of this convective pressure wave will be utilized in the auto- and cross-correlation results discussed in detail in section 6. To demonstrate the validity of this convective pressure pattern, a moving sphere experiment was carried out and the related confirmative results are described in section 4.

To facilitate the interpretation of the correlation method described in sections 5 and 6, the auto-correlation coefficient function for the differential pressure ΔP is included in curve d of figure 4. For a sphere moving at a constant velocity V_∞, the translation between the temporal t and the spatial z coordinates is

$$V_\infty = \frac{z}{t} \qquad [13]$$

In this equation it is assumed that $z = 0$ at tapping 1 and $t = 0$ when the sphere is opposite tapping 1.

From the auto-correlation plot, curve d of figure 4, a clear negative peak 'c' can be identified corresponding to the time τ, which can be used to evaluate the sphere velocity V_∞ as

$$V_\infty = \frac{l}{\tau} \qquad [14]$$

where l is the axial spacing between tappings 1 and 2. As discussed in section 5.1, in a practical experiment the additional peaks a, b and d will be smoothed out due to fluctuations in bubble velocities and deviations in the bubble paths. Consequently, these peaks will not be used for any data correlation.

2.2. *Pressure fluctuations in the continuous phase caused by the continuous phase background turbulence and the wake generated by a bubble*

To estimate the importance of source terms for differential pressure measurements, two parameters must be specified for each source term: the magnitude of the fluctuations and the corresponding correlation length.

A fully developed turbulent single phase water flow was shown to exist within the test pipe (Samways 1992). The magnitude of the continuous phase background turbulence can be described by the turbulence intensity Tu $(=u'/V_L)$, which is about 0.1 near the wall for a fully developed single phase turbulent pipe flow (see e.g. Laufer (1954), Ward-Smith (1980)). The related correlation length is specified by the length scale of the large energy-containing eddies which, in a single phase flow, may vary with flow conditions such as Reynolds number, surface friction factor and entry length. Typically measured values are in the range 0.3–0.9 pipe diameter D (Mitchell & Hanratty 1966, Michiyoshi & Serizawa 1986, Souhar 1989 and Farrar & Bruun 1996). This is comparable to the length scale of the dispersed phase of a two phase-flow which can retain its identity for at least one pipe diameter (Olszowski *et al.* 1976). However, for an average liquid velocity V_L of 0.25 m/s, the corresponding r.m.s. amplitude of the pressure fluctuations ΔP will be of the order of $\Delta P' = \frac{1}{2}\rho_l(0.10V_L)^2 = 0.5$ N/m^2 or 0.05 mm H_2O, which is small compared to the predicted peak magnitude of pressure fluctuations generated by the motion of a single bubble which is of the order of 2–3 mm H_2O.

In a two-phase flow, the presence of bubbles will modify the turbulent structure both in terms of its intensity and correlation length, with the integral length scale of the continuous water phase decreasing with void fraction (Farrar & Bruun 1996).

It has been observed in several experiments that the wake generated behind a bubble as it travels through the continuous phase will increase the turbulence intensity in the continuous water phase (Serizawa *et al.* 1975, Michiyoshi & Serizawa 1986, Wang *et al.* 1987, Lance & Bataille 1991 and Liu & Bankoff 1993a).

Lance and Bataille (1991) found that the (total) turbulent kinetic energy in the continuous phase increases strongly with increasing average gas void fraction $\langle \epsilon \rangle$ and that, broadly speaking, there exists two distinct regimes in which the magnitude of the turbulent kinetic energy of the continuous phase varies. The first is at low average gas void fractions where $\langle \epsilon \rangle$ is less than 1% and the hydrodynamic interaction between bubbles is negligible. Lance and Bataille (1991) found that the second regime occurs at a critical average gas void fraction $\langle \epsilon \rangle_c$ of the order of 1%. In this case the turbulence in the continuous phase is strongly amplified by the hydrodynamic interaction between bubbles.

At even higher void fractions, the interaction between bubbles and continuous phase turbulence is much stronger and highly non-linear. The corresponding effect on the (total) turbulence intensity has been measured in a number of investigations of gas/liquid vertical pipe flows (Serizawa *et al.* 1975, Michiyoshi & Serizawa 1986, Wang *et al.* 1987 and Liu & Bankoff 1993a). In terms of the radial distribution, the highest turbulence intensities were observed in the wall region, with Tu typically reaching 0.15 at high liquid velocities, and values as high as 0.35 have been observed at low liquid velocities (Liu & Bankoff 1993a). This increases the r.m.s. amplitude of the corresponding pressure fluctuations to about 0.5 mm H_2O.

However, for the differential pressure measurements used in this investigation, this increase is cancelled out by a much smaller wake correlation length. If we assume the bubble to be a solid sphere, then the wake generated by a solid sphere in the continuous phase will be of the form of a series of vortex rings (see, for example, Douglas *et al.* 1979). A vortex ring forms for a sphere when the Reynolds number is approximately greater than 10 and becomes unstable at $200 < \mathrm{Re} < 2000$, when it tends to separate from the sphere and is immediately replaced by a new ring. However, unlike a circular cylinder, this process is not periodic and therefore the length scale of these structures will not be constant. Also, the deformation of the bubbles decreases this correlation length even further. Experiments by Lance and Bataille (1991) found that the fluctuations in the bubble wakes become decorrelated within a spatial distance of $0.8d$, which for a bubble diameter of say 6 mm equates to approximately 4.8 mm, which is smaller than the transducer tapping distance used in this investigation (see section 4).

To conclude, for differential pressure measurements in a bubbly two-phase flow, the discussion in this section has shown that the main contributory phenomena to cross-correlation of differential pressure arises from the pressure field of the bubble motion close to the wall, and that the contribution from turbulence in the continuous phase turbulence and bubble wake can be considered small.

3. EXPERIMENTAL FACILITY

A recirculating water flow loop was designed, with a vertical test pipe containing an air bubble injection system. Differential pressure transducers were installed in the vertical test section.

3.1. *Two-phase flow loop*

Figure 5 shows a schematic diagram of the flow loop used in this investigation. The main components of the apparatus comprise a pipe flow loop, air/water separation tank, centrifugal water pump, air injector and the instrumentation used for measuring and controlling the mass flow rates of the two immiscible fluids prior to mixing.

The operation of the flow loop is as follows. Water flows from the separation tank, passes through a filter and enters the centrifugal pump. The pump rotor speed can be adjusted by means of a three-phase thyristor controller, which determines the volume flow rate of water through the test section. A short distance downstream of the flow meter the water turns through a sharp 90° bend and flows vertically upward. This turning introduces a rotational component in its velocity about the axis of flow. To eliminate this, the water passes through a flow straightener prior to air injection and mixing.

Bubbles were formed by air being introduced through a number of small orifices by means of a 'spoked wheel' type air injector with holes of the order of 0.5 mm in diameter along each of the spokes. The air was supplied to the apparatus by a 14 ft^3 min, 10 bar air compressor and regulated

to maintain a constant supply pressure of approximately 1.5 bar. The flow of air into the air/water mixer was regulated by means of a computer controlled needle valve and the mass flow rate of air entering the flow loop was monitored by an orifice plate meter.

The two immiscible phases formed a pseudo-homogeneous flow of bubbles of one phase suspended in the second phase during the passage through a contraction unit prior to entering the vertical test section where the experimental studies were carried out. The contraction was designed by the method of Whitehead *et al.* (1951), which gives a rapid change in cross-sectional area with a small adverse pressure gradient and produces a near uniform velocity profile in the test section. The contraction reduces a 6″ nominal bore pipe to a 3″ nominal bore pipe through a smooth curve.

On leaving the test section, the air/water mixture was delivered to the separation tank via the return pipe, where the two phases separated naturally with the air being exhausted to the atmosphere and the water recirculated.

3.2. *Differential pressure measurements*

3.2.1. *Differential pressure measurements obtained by subtracting two static pressure signals.* This technique was investigated in the present study using two Endevco piezoresistive pressure transducers with a range of 1400 mm H_2O and a response frequency of 70 kHz, which were mounted as near flush as possible with the inside wall of the test section without penetrating into the flow, at a separation distance $l = 25$ mm. Each transducer is internally electrically connected to form a four-active-arm Wheatstone bridge circuit and connected to its own instrument amplifier. The transducers were calibrated using a deadweight tester to give a full range output of 10 V for a maximum pressure of 1400 mm H_2O.

The outputs from the instrument amplifiers were sampled by an A/D converter with a conversion time of 25 μs, with a sampling interval of 100 μs. These two static pressure signals were subtracted digitally to eliminate the common mode component of the signals, leaving only the fluctuating component of the differential pressure signal. Unfortunately, it was found that although this method of measuring differential pressure fluctuations is very simple, implementation of the technique has a number of major drawbacks, such as electronic noise, calibration drift and different response characteristics for the two transducers, as described in Samways (1992).

After extensive trials using two Endevco pressure transducers in the experimental test section of the flow loop, it was decided to investigate the *direct* measurement of the differential pressure signals using a single differential pressure transducer. Then, by comparing the advantages and disadvantages of each technique, an informed decision could be made as to the most suitable transducer configuration for the application under investigation.

3.2.2. *Measurement of differential pressure fluctuations using a single differential pressure transducer.* In this technique two tappings, a short axial distance l apart, are connected to a

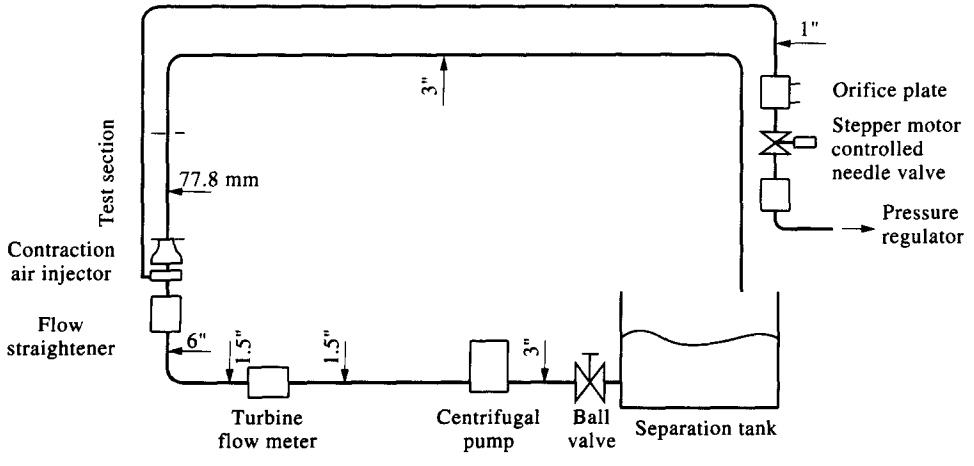

Figure 5. Schematic diagram of the two-phase air/water flow loop.

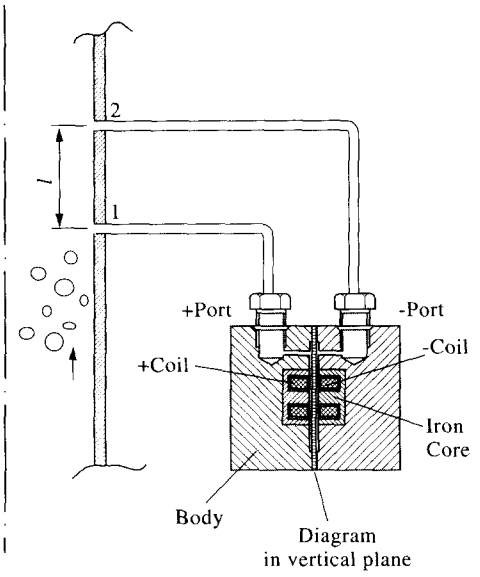

Figure 6. Diagrammatic representation of the single Validyne differential pressure transducer used to investigate differential pressure fluctuations.

differential pressure transducer containing two identical chambers which are separated by a thin diaphragm, as shown in figure 6. Any change in pressure on either side of the diaphragm that is not common to both will cause the diaphragm to be displaced. Over the operational range of the transducer, the displacement will be linearly proportional to the differential pressure between the two tappings. A single Validyne DP15 differential pressure transducer with a number 22 diaphragm, which has a range of ± 140 mm H_2O, was initially connected, using nylon pipes, to two tappings in the test section separated by an axial distance $l = 25$ mm. The diaphragm of the transducer was positioned in the vertical plane as shown in figure 6, in order to eliminate any gravitational effects.

For use in water flows it is necessary to bleed the air from the transducer and the associated pressure lines. This proved to be very difficult due to the internal design of the transducer pressure chambers, which it is thought were designed for gases. Also, it was found that any vibration of the nylon pressure lines resulted in the fluid contained within these pipes being displaced, thus causing inertia forces to act on the diaphragm. The inertia forces of the water in the pressure lines generated far greater differential pressure fluctuations than those caused by the bubbles. To reduce the magnitude of this effect, the nylon pressure lines were replaced by much stiffer pressure lines manufactured from copper. This reduced the magnitude of the noise fluctuations but not sufficiently to make this transducer arrangement a satisfactory one.

Solid transducer mounting: to minimize the problems of vibrations, it was decided to design and manufacture a solid transducer mounting facility from aluminium alloy. This contained not only the pressure lines from the wall tappings to the differential pressure transducer, but also acted as a rigid mounting for the pressure transducer, as can be seen in figure 7. The housing was designed to be robust, in order to eliminate independent vibration of components, and to facilitate the bleeding of air from the system. By incorporating the pressure lines into a solid body, any system vibration will be common to both sides of the transducer diaphragm and so, to a large extent, will therefore cancel each other out.

To facilitate the bleeding of air from the transducer and the associated pressure lines, all pressure lines have been reamed to make them smooth and machined at an angle to allow the air to bleed out naturally. Screw threads in pressure line fittings can also trap air, therefore all bleed ports have been sealed using blanking plates rather than screw plugs. The internal bore of the transducer housing is the same as the bore of the test section (77.8 mm), and it was designed to fit between two flanges. The housing was positioned approximately 0.6 m downstream from the contraction

in approximately the middle of the experimental test section. Two axially in-line pressure tappings 1 mm in diameter are separated by a distance l of 25 mm.

3.3. *Modifications of experimental apparatus used to measure differential pressure fluctuations for use in cross-correlation flow measurement techniques*

For cross-correlation experiments to be performed, *two* differential pressure signals $\Delta P_A(t)$ and $\Delta P_B(t)$ are required, arranged as shown in figure 8 where $\Delta P_A = P_1 - P_2$ and $\Delta P_B = P_3 - P_4$, where P_1 through P_4 are the wall pressure tappings. Note that the wall pressure tappings need to be axially in line since the pressure tapping-to-bubble centre separation distance can affect the magnitude of the pressure signal generated by the motion of a bubble. The transducer separation distance h between the two differential pressure transducers A and B has been chosen to be 6 mm, which is of the order of a single bubble diameter.

Based on these preliminary experiments, modifications to the existing differential pressure transducer housing were made to accommodate a second differential pressure transducer B with pressure tappings 3 and 4 positioned 6 mm downstream of the tappings 1 and 2 respectively, as shown in figure 8.

In situ calibration was conducted on the two differential pressure transducers, the aluminium housing and the experimental test section, were all subjected to the same simultaneous excitation vibration after being mounted in position in the flow loop. The vibrations were generated by a rotating eccentric mass mounted on the supporting framework of the test section. From initial impact hammer frequency tests, it was found that a Validyne pressure transducer and housing had a frequency response of the order of 400 Hz. This is much lower than the Endevco pressure transducers. However, Matsui (1984) and others have found that the frequency spectrum of a pressure signal from a bubbly two-phase flow with superficial gas and liquid velocities in the range covered in the present study contains little energy at frequencies higher than 100 Hz.

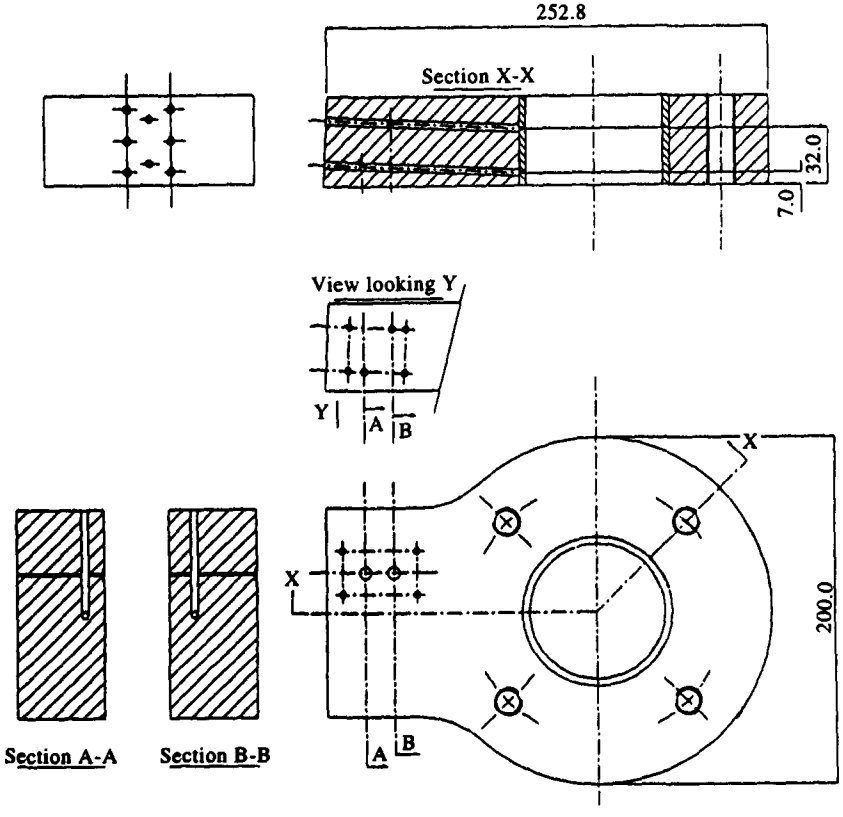

Figure 7. Housing/mounting facility for Validyne differential pressure transducer.

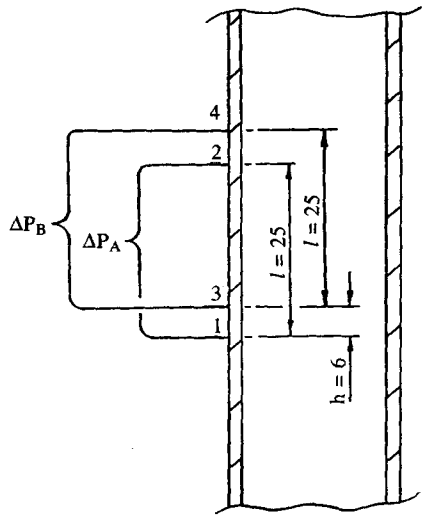

Transducer tapping arrangment for cross correlation measurements

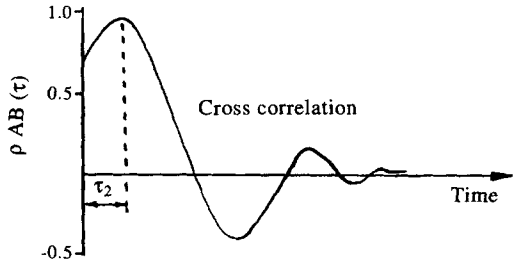

Figure 8. Arrangement of the differential pressure tappings 1, 2, 3 and 4 used to measure ΔP_A and ΔP_B and the interpretation of a typically measured cross-correlation coefficient function.

After considering the advantages and disadvantages of both methods, it was decided that the most suitable technique for use in this application would be the Validyne differential pressure transducer method.

4. COMPARISON OF THEORETICAL AND EXPERIMENTAL PRESSURE FLUCTUATIONS

A solid sphere experiment was designed to make comparisons between theoretical differential pressure fluctuations, derived from Butler's sphere theorem in section 2, and measured differential pressure fluctuations. Differential pressure fluctuations were measured and calculated for a sphere moving at constant velocity through a stagnant column of liquid in a pipe. From the results of these experiments, conclusions were drawn about the validity of modelling the bubbles as solid spheres.

Although the experiment was carried out in stagnant water, where there is no continuous phase background turbulence, the effect of the continuous phase turbulence is expected to result in only a slightly higher magnitude of measured differential pressure fluctuations. Although the length scale of structures in the background turbulence may be of the order of the pipe diameter, they are not, as discussed in section 2.2, expected to have much of an effect on the main feature of the auto-correlation function of differential pressure fluctuations, since the magnitude of the background turbulence pressure fluctuations is small when compared to the main convected pressure fluctuation field in a bubbly two-phase flow.

4.1. *Experimental differential pressure fluctuations caused by a moving sphere in a pipe containing stagnant water*

A 6.5 mm diameter solid sphere was attached to a thin nylon cord and strung between two pulleys as shown in figure 9. Attached to this nylon cord loop was a second nylon cord which was wound around a pulley fixed to a stepper motor. The sphere was strung tightly between the two fixed pulleys and could therefore only move along the fixed path at constant velocity. Knowing the diameter of the pulley fitted to the stepper motor, the frequency of the pulse train supplied to the stepper motor corresponding to various constant bead (sphere) velocities could be calculated.

The sphere apparatus described above was positioned in a short section of transparent pipe similar to that used in the test section of the flow loop. The transducer housing with a single Validyne differential pressure transducer attached, used to measure differential pressure fluctuations in the experimental test section, was also positioned in this section of pipe.

The combined short test section was set up and the air bled from the differential pressure transducer. The required stepper motor frequencies were calculated to drive the sphere at constant velocities of 0.1, 0.25, and 0.4 m/s. The output from the differential pressure transducer amplifier was connected to a Bruel & Kjaer model 2034 dual channel analogue signal analyser, which interfaced the output from the Bruel & Kjaer's IEEE488 parallel port with a similar port on an IBM compatible computer.

Differential pressure fluctuations were measured for wall-to-sphere centre separations ranging from 4.5–25.5 mm at the three constant sphere velocities. A typical measured differential pressure signal corresponding to an axial separation l of 25 mm normalised using $\frac{1}{2}\rho_l V_b^2$ is shown in figure 10, for a wall-to-sphere centre distance of 4.5 mm, at a constant sphere velocity of 0.25 m/s. Also plotted in figure 10 is the predicted shape of the related normalised pressure wave caused by the motion of a sphere derived from [11] (Butler's sphere theorem in section 2). It is noticed that for this condition the maximum amplitudes of the measured and calculated pressure fluctuations are similar. Variations observed between the calculated and measured pressure signals may be due to the influence of the pipe wall and the wake generated by the moving sphere on the measured signal, which is not accounted for in the theoretical calculations. Although the measured differential pressure wave from the constant velocity bead experiment is not as well defined, and generally the

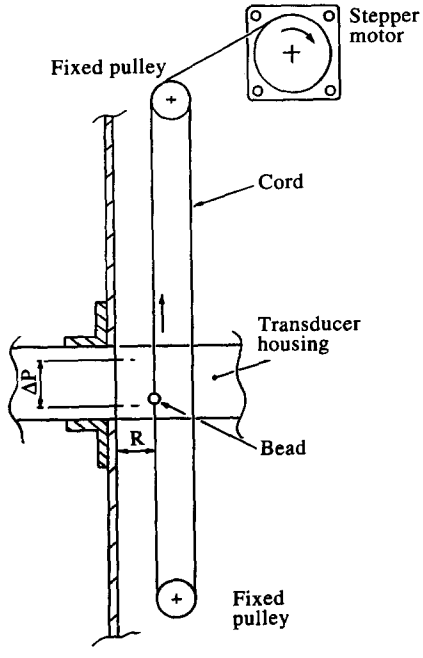

Figure 9. Experimental apparatus used to measure differential pressure fluctuations generated by the motion of a sphere in a stagnant column of water.

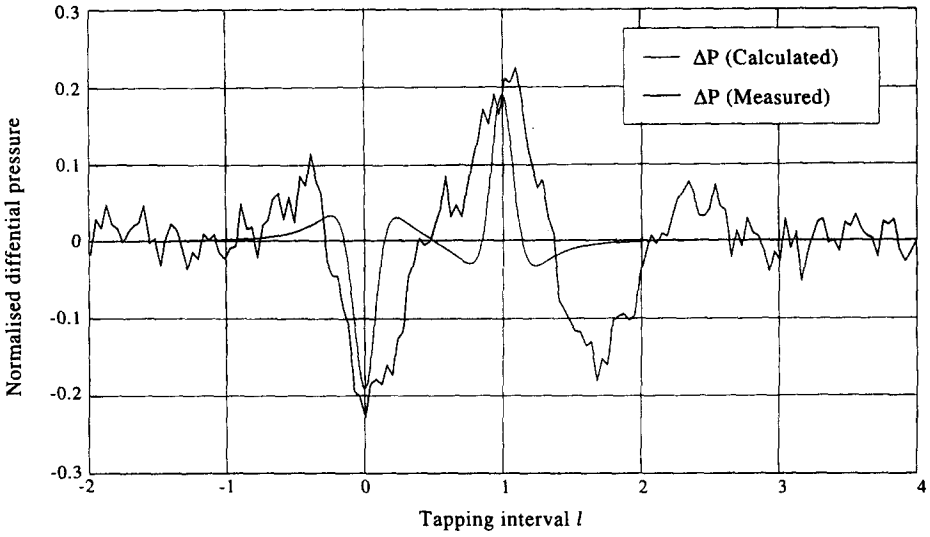

Figure 10. Differential pressure signal measured in moving sphere experiment and corresponding theoretical prediction from [11]. The experimental and theoretical pressures correspond to a moving sphere of diameter 6.5 mm travelling with a constant velocity of 0.25 m/s at a wall-to-sphere centre separation distance of 4.5 mm.

peaks are broader than the calculated pressure wave, the peak pressures occur at the same time (or space) location for both measurements and experiments. This demonstrates the ability of the correlation technique (section 5) to evaluate bubble velocities.

Experiments were carried out using values of the ratio between the pipe wall-to-sphere centre separation distance over a sphere radius R/a between 1.5 and 7, and with three constant sphere velocities 0.1, 0.25 and 0.4 m/s. In general, similar results were obtained in all cases, with the peak pressures occurring at the same time for both measurements and experiments and with similar peak pressure values.

5. THE DIFFERENTIAL PRESSURE CORRELATION PRINCIPLE

The convected pressure field was recorded at pressure tappings separated in the longitudinal direction by a distance l in the vertical pipe. To facilitate the interpretation of the experimental results in section 6, the following conclusions concerning the pressure field surrounding a single moving bubble should be noted.

The pressure fluctuations generated by variations in the pressure field surrounding a moving bubble (see section 2.1) rapidly diminish in amplitude with increasing distance from the bubble and become insignificant at distances greater than 3–4 bubble diameters. This means that for bubbles further than 3–4 bubble diameters d from a pressure transducer tapping, no contribution will be detected that can be associated with the bubble's motion. This information can be applied to two pressure tappings 1 and 2, separated by a distance $l \geqslant 4d$ in the flow direction, and connected to a differential pressure transducer A. It should be noted that in the experimental study a typical value for d was 6 mm, and with $l = 25$ mm this condition was satisfied.

The corresponding differential pressure is denoted $\Delta P_A(t) = P_1(t) - P_2(t)$. If at any time t_1 a single bubble is located close to pressure tapping 1, then $P_1(t_1)$ will record the convected pressure associated with a distortion in the pressure field surrounding this bubble, caused by its motion, while the corresponding pressure at point 2, $P_2(t_1)$, will be unchanged since point 2 is more than $4d$ away. If we assume the bubble moves with a velocity V_∞ in a straight line past the tapping points 1 and 2, then at a later time t_2, tapping 2 will record the convected bubble pressure signal $P_2(t_2)$, while the corresponding signal at 1, $P_1(t_2)$, will now be unaffected by this bubble.

5.1. *Auto-correlation*

The ideal frozen pattern auto-correlation of the differential pressure from a single bubble, illustrated by curve d in figure 4, is for comparative purposes also reproduced in figure 11 as curve a. When ΔP_A is evaluated for the integrated effect of many bubbles (which may not all be travelling at exactly the same velocity), then the form of the experimentally measured auto-correlation will conform to a diffused correlation model as shown by curve b in figure 11. From this figure, a convected bubble velocity V_{G1} can be evaluated as

$$V_{G1} = \frac{l}{\tau_1} \qquad [15]$$

5.2. *Cross-correlation*

These results were obtained using two differential pressure transducers A and B, with A connected to pressure tappings 1 and 2 and B connected to 3 and 4, as shown in figure 8. As can be seen, transducer B is shifted by a small distance h in the flow direction relative to transducer A. The two sets of pressure tappings 1, 2 and 3, 4 for each differential pressure transducer have the same tapping separation distance $l = 25$ mm. In the present study the transducer separation distance h of 6 mm has been chosen, which is of the order of one bubble diameter d in this study. The cross-correlation of the signal from pressure transducer A with that from pressure transducer B produces a correlogram of the form shown in figure 8. A convected bubble velocity V_{G2} can be evaluated from the cross-correlation function which corresponds to the correlation length scale of the shorter transducer separation distance $h = 6$ mm. The corresponding convected bubble velocity can be evaluated as

$$V_{G2} = \frac{h}{\tau_2} \qquad [16]$$

where τ_2 is the time delay associated with the convected bubble velocity V_{G2}, evaluated from the cross-correlation function shown in figure 8.

Over the short distance h, deviation from a frozen pattern will be considerably smaller compared to that measured over the tapping separation distance l, which is approximately four bubble diameters. However, the velocity and trajectories of bubbles within a bubbly two-phase flow may affect the convected bubble velocity evaluated by V_{G1} and V_{G2} in the following way.

It is well known that bubbles wander in a spiralling motion during their ascent through an unbounded fluid. Results from Moursali *et al.* (1995) have shown that a typical bubbly two-phase flow exhibits migration of bubbles towards the test section wall where some are entrapped within a layer near the wall while others appear to travel into the layer and then 'bounce' away on a

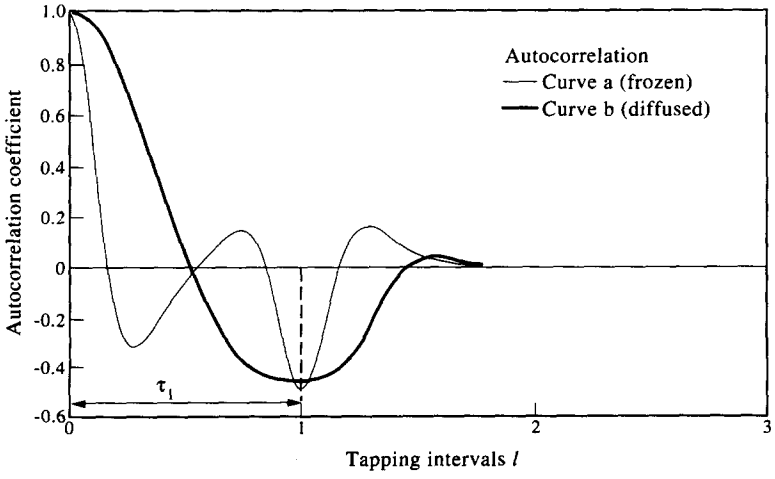

Figure 11. Frozen and diffused pattern auto-correlations of pressure fluctuations within a bubbly two-phase flow.

new trajectory. If a bubble's velocity and size are similar to those of other bubbles near the wall, then the bubble becomes entrapped in the layer near the wall causing the characteristic high local void fraction region near the test section wall. It was also noticed that bubbles that 'bounce' away from the wall are both larger and travel at higher velocities than those entrapped near the wall.

The effect of these observations by Moursali *et al.* (1995) on the convected auto-correlation velocities V_{G1}, evaluated over the longer 25 mm correlation length scale, will be that the faster moving bubbles which do not remain near the pipe wall, i.e the bubbles that 'bounce' away will have little or no effect on the corresponding evaluation of the convected bubble velocity. This is because a bubble that moves in and out of the entrapped bubble layer will do so in an axial distance which is much shorter than the correlation length scale of 25 mm. However, a faster moving bubble, which generates a higher magnitude of pressure fluctuation, will effect the convected bubble velocity V_{G2}, which is evaluated over the shorter 6 mm length scale, if it enters and leaves the entrapped bubble layer near either pressure tappings 1 and 3, or 2 and 4. Consequently the evaluated convected bubble velocity V_{G2} is expected to be higher than the convected bubble velocity evaluated from the auto-correlation V_{G1}, but lower than the velocity of bubbles which remain in the main flow.

5.3. *Previous bubbly two-phase flow correlation techniques*

Cross-correlation of fluctuations in a bubbly two-phase flow at location 1 with another location 2 further downstream have been attempted by a number of researchers. The most common technique involves the monitoring of fluctuations in the average void fraction at points 1 and 2. Cross-correlation of these two signals is then normally utilized to evaluate the area averaged convected disturbance velocity V from the known distance l between the measuring locations and the time shift τ of the correlation peak

$$V = l/\tau \qquad [17]$$

Fluctuations in the average void fraction can be monitored by a number of techniques such as ultrasonic (Matthes *et al.* 1970, Olszowski *et al.* 1976, Ong 1975, Xu 1986), impedance (Bernier 1981 and Kyatomaa 1987), capacitance (Hammer 1983 and Lucas 1987) and differential pressure fluctuations (Matsui 1984).

However, conflicting convected dispersed phase velocity results have been observed from these techniques, and reasons for discrepancies are discussed below.

It is well known that within a bubbly two-phase flow there will exist both a local void fraction profile and a corresponding local dispersed phase velocity profile across the test section. As shown by e.g. Serizawa *et al.* (1975), Wang *et al.* (1987) and Liu and Bankoff (1993b), typical bubbly two-phase flow tends to show regions of high local void fraction near the test section walls caused by migrating bubbles becoming entrapped within a layer at the pipe wall.

Typical corresponding local dispersed phase velocity profiles have been reported by Serizawa *et al.* (1975) and Liu and Bankoff (1993a) and these results indicate that bubbles near the pipe wall travel significantly more slowly than bubbles near the centre of the test section. The reason for this velocity profile is thought to be primarily due to friction effects at the pipe wall where the velocity of the continuous phase approaches zero. If we therefore consider a bubble which is travelling close to the pipe wall, its velocity will be less than the area averaged dispersed bubble velocity, similarly if a bubble is away from the wall near the centre of the pipe, its velocity will be greater than the area averaged velocity.

Returning then to the case of the dispersed bubble velocity measurements evaluated from the cross-correlation of void fraction fluctuations, with the above description of a bubbly two-phase flow in mind, it is not difficult to appreciate that if the void fraction transducer being used to monitor fluctuations performs in a way that spatially filters the flow within the pipe, i.e. the transducer does not have a uniform sensitivity and is therefore more sensitive to a particular region or event within the flow, then the result of cross-correlating such signals will be to reflect the velocity of disturbances within this region or event (see Hammer and Green (1982)). For example, consider a void fraction monitoring transducer with a non-uniform sensitivity across the diameter of the test section, which is more sensitive to fluctuations in the void fraction nearer the centre of the

test section. Then cross-correlation of signals from two such transducers will result in the evaluation of a higher than average dispersed bubble velocity. Similarly if the transducer is more sensitive to fluctuations near the pipe wall, this will be reflected in the evaluation of lower than area averaged dispersed bubble velocities. The spatial filtering effect may also be extended to cover void fraction monitoring transducers that are more sensitive to particular ranges of void fractions, such as high or low, and therefore cross-correlation of these signals will reflect the velocity of bubbles within that particular void fraction region.

Consider capacitance void fraction monitoring transducers. Lucas (1987) cross-correlated the measurements of two axially separated, so termed 'uniform field strength' capacitance transducers in vertically upward bubbly air/water two-phase flow within a test section with diameter $D = 77.8$ mm. In this study, the axial separation l between the two transducers was 160 mm or $l \approx 2D$. Cross-correlation of the two signals produced correlograms whose peak positions were used to evaluate the transit time of the signal τ, and the corresponding convection velocity was evaluated using [17]. Similar measurements were also carried out by Hammer (1983).

The cross-correlation convected bubble velocities were compared with high speed serial photography of the bubbly two-phase flows, and area averaged gas velocity calculated from [20]. Lucas found that in vertically upward bubbly two-phase flows, the convection velocity obtained by his cross-correlation measurement technique gave results which were always in *excess* of the actual area average dispersed phase velocity. Both Hammer (1983) and Lucas (1987) accounted for their respective discrepancies in the measured area averaged bubble velocities by suggesting that their respective capacitance transducers are more sensitive to detecting larger faster moving bubbles in the centre of the flow which are generally travelling quicker than the actual area averaged bubble velocity.

However, different results have been obtained with impedance monitoring void fraction transducers. Bernier (1981) carried out experiments in which he attempted to measure the average velocity of structures in vertically upward bubbly air/water two-phase flows using two flush mounted impedance transducers, which were axially separated by a distance l, and he found, in contradiction to Hammer (1983) and Lucas (1987), that evaluated cross-correlation velocities were always lower than the actual area averaged bubble velocity. Kyatomaa (1987) using the same flow loop as Bernier conducted a series of cross-correlation experiments using virtually identical impedance transducers to Bernier, except Kyatomaa employed shielding electrodes on either side of the measurement electrodes. Kyatomaa's experiments tend to confirm Bernier's findings, and both agree that their impedance cross-correlation measurements in bubbly two-phase flows reflect the propagation velocity of the infinitesimal kinematic waves and not the area averaged velocity of the dispersed bubbles.

In the study by Bernier, he assumes the flow to be both one-dimensional and under steady state conditions. In Bernier's analysis of a theoretical bubbly two-phase flow, he considered the possibility of a long section of flow, at any instant in time, being divided up into discrete regions of constant average gas void fraction, however, the value of average gas void fraction within each region may vary from region to region. These regions of constant average gas void fraction, he suggests, are separated by structures in the flow and from experimental work he concludes that his impedance cross-correlation technique does not measure the area average bubble velocity of the flow but actually measures the velocity of these slower moving, large scale structured waves, which he termed 'infinitesimal kinematic waves'.

Bernier (1981) suggested that his 'infinitesimal kinematic waves' are similar to those of Lighthill and Whitham (1955), in which the propagation of traffic flow disturbances along major arterial roads was studied. An analogy can be drawn between discrete bubbles flowing along a pipe in a bubbly two-phase flow and discrete cars all travelling in the same direction along a crowded road. It was reported by Lighthill and Whitham that the propagation speed of a kinematic wave will be less than the average velocity of the vehicles, and similarly in a fluid kinematic waves travel slower than the area averaged velocity of the fluid. In vertical bubbly two-phase flow, bubbles travelling at a terminal velocity greater than the kinematic wave propagation speed, on reaching the rear of the kinematic wave, slow down fairly rapidly. After travelling through the wave the bubbles can only increase their speed gradually. This results in a concentration in void fraction

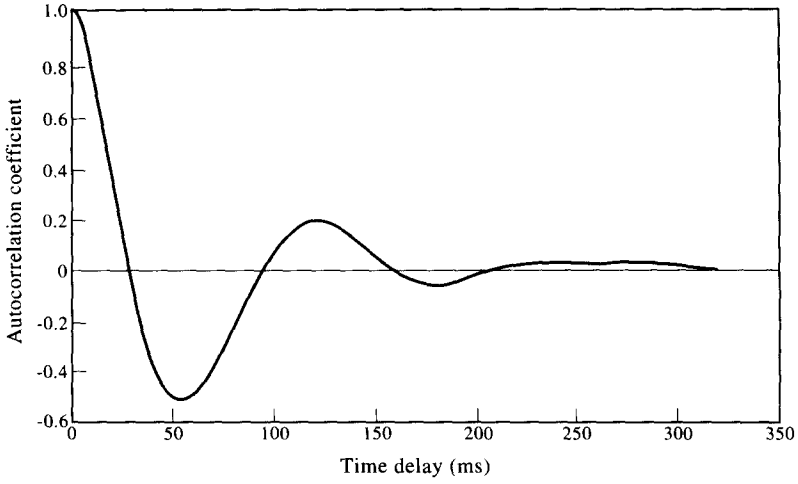

Figure 12. Measured auto-correlation of differential pressure fluctuations, $V_{SL} = 1.0$ m/s, $\langle \epsilon \rangle = 10\%$.

around the wave and consequently causes dense and sparse regions of gas void fraction within the bubbly two-phase flow.

Although Bernier (1981) and Kyatomaa (1987) concluded that they are measuring the kinematic wave speed and not the area averaged bubble velocity, the discrepancies observed between the evaluated cross-correlation velocity and the actual area averaged bubble velocity can also be explained from a spatial filtering point of view. For example, if their respective impedance monitoring void fraction transducers do not have a uniform field sensitivity and are more sensitive to the slower moving bubbles near the pipe wall, filtering out the faster moving bubbles near the centre of the pipe, then the cross-correlation velocity will reflect the velocity of the bubbles near the pipe wall. Since these bubbles tend to travel slower than the area averaged bubble velocity, this could also account for the discrepancies observed by Bernier (1981) and Kyatomaa (1987).

Finally, Matsui (1984) investigated cross-correlation of two differential pressures ΔP_a and ΔP_b for the spherical-cap bubble flow regime, as discussed in section 1.

In concluding this section, it should be remembered that the transducer separation distances l used by Bernier (1981), Kyatomaa (1987), Hammer (1983), and Lucas (1987) were all on the order of two pipe diameters, $l \approx 2D$, which is much larger than found acceptable in this study (see section 3). This would indicate that impedance and capacitance void fraction measuring transducers are more sensitive to much larger scale structures in the bubbly two-phase flow than those being detected in the present study using differential pressure fluctuations.

6. EXPERIMENTAL RESULTS

6.1. *Initial experimental auto-correlations from a single differential pressure transducer*

Using a single differential pressure transducer and housing as described in section 3, positioned in the experimental test section of the flow loop approximately 0.6 m downstream of the contraction, differential pressure measurements $\Delta P_A(t)$ have been made as a function of time t, over a range of superficial gas and liquid velocities, V_{SG} and V_{SL} respectively. Average gas void fractions $\langle \epsilon \rangle$ were also recorded simultaneously. Auto-correlation correlograms of the recorded differential pressure signals were obtained for superficial liquid velocities V_{SL} of 0, 0.64, 1.0 and 1.5 m/s, each with an average gas void fraction $\langle \epsilon \rangle$ of approximately 10%. The pressure signals were a.c. coupled, and therefore the auto-correlations generated are for the fluctuating component of the differential pressure signal only.

A typical auto-correlation result is shown in figure 12. It should be noted that the magnitude of the auto-correlation coefficient, $\rho_{AA}(\tau)$, when the pressure signal is in complete anti-phase is approximately -0.45, indicating a high degree of correlation over the time τ_1.

The time τ_1 (defined by figure 11) taken for the experimental auto-correlation correlograms to reach complete anti-phase was found to be almost constant. The convected bubble velocity V_{G1}, which was calculated from [15], ranged from 0.40 m/s for bubbles travelling through a stagnant column of water to 0.51 m/s for bubbles travelling through water which had a superficial liquid velocity V_{SL} of 1.5 m/s.

6.2. *Experimental results obtained from auto- and cross-correlation correlograms*

A series of experiments was also undertaken using two differential transducers as explained in section 3.

Auto-correlation correlogram $\rho_{AA}(\tau)$ and $\rho_{BB}(\tau)$ results from both the upstream and downstream differential pressure transducers A and B respectively were recorded along with the cross-correlation correlogram $\rho_{AB}(\tau)$. The range of superficial gas and liquid velocities V_{SG} and V_{SL} was 0.018–0.35 m/s and 0–1.5 m/s respectively, covering a range of average gas void fractions $\langle\epsilon\rangle$ of approximately 5%–25%. The superficial gas and liquid velocities were evaluated from

$$V_{SG} = \frac{\dot{V}_G}{A} \qquad [18]$$

$$V_{SL} = \frac{\dot{V}_L}{A} \qquad [19]$$

where $\dot{V}_G$ and $\dot{V}_L$ are the gas and liquid volume flow rates respectively and A the cross-sectional area of the pipe using information from the air mass flow rate orifice meter and the water turbine flow meter. The average gas void fraction $\langle\epsilon\rangle$ was continuously monitored using the gradiomanometer technique described by Hunt (1987) and Samways (1992), and it has the advantage over the rapid closing gate valve technique in that it is non-intrusive to the flow. In can therefore be used to measure the average gas void fraction whilst experiments are being carried out in the test section.

The area averaged gas velocity V_G, of bubbles in the experimental test section was calculated using

$$V_{SG} = \langle\epsilon\rangle V_G \qquad [20]$$

from the superficial gas velocity V_{SG}, and the average gas void fraction $\langle\epsilon\rangle$.

The axial separation of the pressure tappings from the two differential pressure transducers A and B is, as explained earlier, shown in figure 8.

In the analysis of these experiments we have assumed that $l_A = l_B = 25$ mm, and therefore only the auto-correlations of ΔP_A have been considered when evaluating the convected bubble velocity V_{G1}. It has also been assumed that pressure tapping 3 is exactly 6 mm downstream of pressure tapping 1, when calculating the bubble velocity V_{G2}.

Experiments were carried out with both zero continuous (water) phase flow and with continuous phase flow in the pipe.

6.2.1. *Zero continuous phase velocity*. The most striking difference between the two cases was observed for the cross-correlation and consequently in the corresponding convected bubble velocities V_{G2}, evaluated for the stagnant water column, $V_L = 0$, compared with those evaluated when the continuous phase is flowing ($V_L \neq 0$).

A typical set of auto- and cross-correlation results is shown in figure 13. The convected bubble velocity V_{G1}, evaluated from the auto-correlation over the 25 mm correlation length scale, was found to be almost constant with a value of approximately 0.38 m/s. Interpretation of the convected bubble velocity V_{G1} in section 5.1. indicates that V_{G1} reflects the velocity of bubbles travelling close to the pipe wall. This indicates that small bubbles 'stick' to the wall region even for the stagnant water flow case.

The convection velocity V_{G2} evaluated from the cross-correlation over the 6 mm correlation length scale gives convected bubble velocities V_{G2}, which from the arguments put forward in section 5.2 are expected to be influenced by the velocity of bubbles which wander close to the pipe wall and then deviate away. The measured results indicate a convection velocity of these bubbles of approximately 0.6 times the area averaged gas velocity V_G. However, the magnitude ($\sim$0.1–0.2)

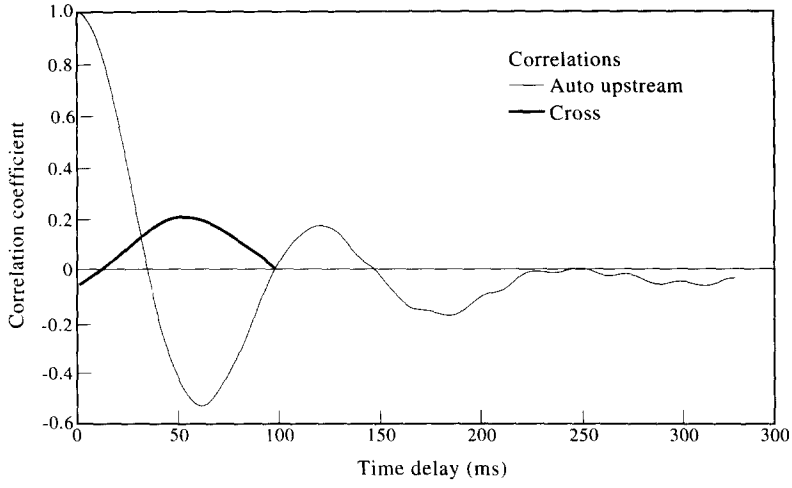

Figure 13. Measured auto- and cross-correlation functions of differential pressure fluctuations in bubbly flow. Stagnant water, $V_{SL} = 0$ m/s, $\langle \epsilon \rangle = 10\%$.

of the cross-correlation coefficient is so low that no consistent bubble motion can be identified. One reason for this greater diffusion effect to be observed in the zero continuous phase flow conditions will be the absence of an entrapped bubble layer near the pipe wall due to a reduced lift force acting on bubbles as they ascend through a stagnant continuous phase, therefore not causing bubbles to migrate towards the wall.

6.2.2. *With continuous phase flow*. A typical set of auto- and cross-correlation coefficient results is shown in figure 14.

Analysing the data for conditions other than zero continuous phase flows, it was found that the auto-correlation convected bubble velocity V_{G1} changed little from 0.41 m/s at $V_{SL} = 0.5$ m/s to 0.47 m/s at $V_{SL} = 1.5$ m/s over the range of superficial liquid velocities covered in this study (0.5–1.5 m/s). This indicates that bubbles near the pipe wall are travelling at a constant velocity of approximately 0.4 m/s, consistent with the velocity of bubbles close to the pipe wall travelling much slower than the area averaged or free stream bubble velocity.

The cross-correlation coefficient was found to have a high maximum value ranging from about 0.7 at a superficial liquid velocity V_{SL} of about 0.5 m/s to 0.9 at $V_{SL} \approx 1.5$ m/s. This increase in the

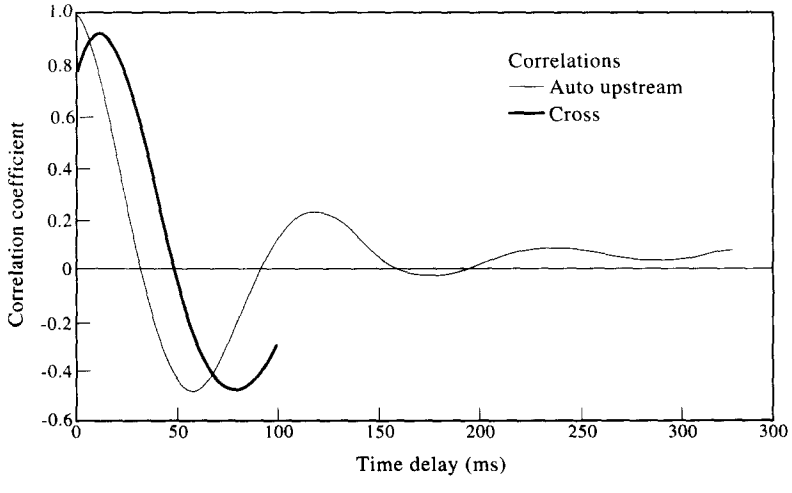

Figure 14. Measured auto- and cross-correlation functions of differential pressure fluctuations in bubbly flow, $V_{SL} = 0.5$ m/s, $\langle \epsilon \rangle = 20\%$.

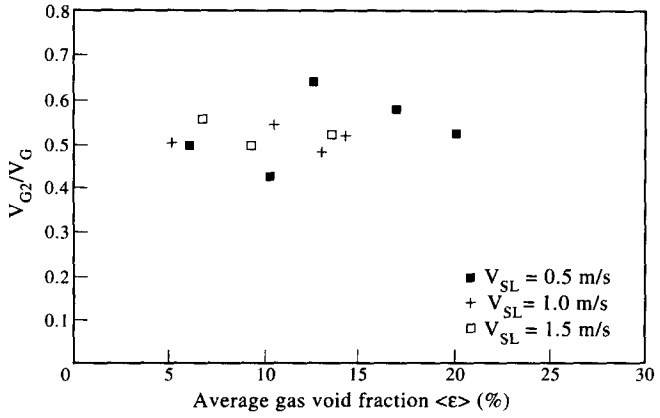

Figure 15. Measured values of convected disturbance velocity ratio V_{G2}/V_G, based on transducer separation $h = 6$ mm plotted for non-zero continuous phase flows as function of the average gas void fraction $\langle \epsilon \rangle$.

peak value indicates the retention of faster moving bubbles in the wall boundary layer over longer axial distances with increasing liquid velocity.

The results for the convected bubble velocity V_{G2} defined in [16] evaluated over the shorter 6 mm correlation length scale are plotted as the ratio V_{G2}/V_G, in figure 15 as a function of the average gas void fraction $\langle \epsilon \rangle$. These ratios can be seen to exhibit some scatter ranging from 0.640 as a maximum to 0.427 as a minimum with an average of 0.55. The ratio V_{G2}/V_G can be seen to be almost constant (approximately 0.55) over the continuous phase velocity range considered in this study, which indicates that the convected bubble velocity V_{G2} is influenced by the velocity of the continuous phase, whereas the corresponding auto-correlation convected bubble velocities V_{G1}, are not, and remain almost constant at approximately 0.4 m/s. This suggests that correlation velocities of convected disturbances evaluated over the 25 mm correlation length scale, i.e. V_{G1}, reflect the almost constant velocity of entrapped bubbles near the wall ($V_{G1} \approx 0.4$ m/s), whereas convection velocities evaluated over the shorter 6 mm correlation length scale, i.e. V_{G2}, are influenced by faster moving bubbles than those at the pipe wall and the convected bubble velocity V_{G2} reflects a velocity which is approximately 0.55 that of the area averaged bubble velocity V_G.

7. CONCLUSION

This study has investigated the use of pressure fluctuations caused by the dispersed (bubbly) phase of a two-phase flow for bubble velocity measurements.

On the experimental side, a substantial effort was devoted to the development of a reliable differential pressure transducer technique for the study of convected pressure fields related to bubble motion.

Related theoretical derivations and experiments with a moving sphere conclusively proved that a differential pressure transducer technique could be used to measure the convected pressure field of bubbles travelling close to the wall.

Detailed measurements with a single differential pressure transducer housing an axial pressure tapping separation of 25 mm and two differential pressure transducers with an axial spacing of 6 mm were carried out. Related auto- and cross-correlation measurements demonstrated that the axial separation of 25 mm identified slow moving bubbles which travel in the 'entrapment' layer next to the wall. The measured bubble convected velocity ($V_{G1} \approx 0.4$ m/s) was found to be nearly independent of the superficial liquid velocity V_{SL} in the range 0.5–1.5 m/s. For the shorter axial separation $h = 6$ mm, the dual transducer cross-correlation technique identified faster moving bubbles which move into the entrapment layer and then bounce away again. For these bubbles, the corresponding convection velocity ratio V_{G2}/V_G was found to be nearly constant (≈ 0.55), independent of superficial liquid velocity and gas void fraction.

Acknowledgements—A. L. Samways wishes to acknowledge financial support and provision of equipment from Schlumberger Cambridge Research Ltd.

REFERENCES

Bernier, R. J. N. (1981) Unsteady two-phase flow instrumentation and measurement. Report No. E200.4, Division of Engineering and Applied Science, California Institute of Technology.

Butler, S. F. J. (1953) Sphere theorem. *Proc. Camb. Philos. Soc.* **49,** 169–174.

Douglas, J. F., Gasiorek, J. M. and Swaffield, J. A. (1997) *Fluid Mechanics*. Pitman Books Ltd., London, ISBN 0-27300-462-X.

Farrar, B. and Bruun, H. H. (1996) A computer based hot-film technique used for flow measurements in a vertical kerosene–water pipe flow. *Int. J. Multiphase Flow* **22,** 733–751.

Hammer, E. A. (1983) Three component flow measurement in oil/gas/water mixtures using capacitance transducers. Ph.D. Thesis, University of Manchester.

Hammer, E. A. and Green, R. G. (1982) The spatial filtering effect of capacitance transducer electrodes. *J. Phys. E.: Sci. Instrum.* **16,** 438–443.

Hunt, A. (1987) The Venturi meter – theory. Report prepared for Schlumberger Cambridge Research, Cambridge.

Kyatomaa, H. K. (1987) Stability of the structure in multicomponent flows. Report No. 200.24, Dept of Applied Science, California Institute of Technology.

Lance, M. and Bataille, J. (1991) Turbulence in the liquid phase of a uniform bubbly air-water flow. *J. Fluid Mech.* **222,** 95–118.

Laufer, J. (1954) The structure of turbulence in fully developed pipe flow. NACA Report 1174.

Lighthill, M. J. and Whitham, G. B. (1955) On kinematic waves II. A theory of traffic flow on long crowded roads. *Proc. Roy. Soc.* **229A,** 317–345.

Lucas, G. P. (1987) The measurement of two-phase flow parameters in vertical and deviated flow. Ph.D. Thesis, University of Manchester.

Lui, T. J. and Bankoff, S. G. (1993a) Structure of air–water bubbly flow in a vertical pipe I. Liquid mean velocity and turbulence measurements. *Int. J. Heat Mass Transfer* **36,** 1049–1060.

Lui, T. J. and Bankoff, S. G. (1993b) Structure of air–water bubbly flow in a vertical pipe II. Void fraction, bubble velocity and bubble size distribution. *Int. J. Heat Mass Transfer* **36,** 1061–1072.

Matsui, G. (1984) Identification of flow regimes in vertical gas–liquid two-phase flow using differential pressure fluctuations. *Int. J. Multiphase Flow* **10,** 711–720.

Matthes, W., Riebold, W. and deCooman, E. (1970) Measurement of the velocity of gas bubbles in water by a correlation method. *Rev. Sci. Instrum.* **4,** 843–845.

Michiyoshi, I. and Serizawa, A. (1986) Turbulence in two-phase bubbly flow. *Nucl. Eng. Des.* **95,** 253–267.

Milne-Thomson, L. M. (1960) *Theoretical Hydrodynamics*, 4th edn. MacMillan & Co. Ltd., London.

Mitchell, J. E. and Hanratty, T. J. (1966) A study of turbulence at a wall using an electrochemical wall shear-stress meter. *J. Fluid. Mech.* **26,** 199–221.

Moursali, E., Marie, J. L. and Bataille, J. (1995) An upward turbulent bubbly boundary layer along a vertical flat plate. *Int. J. Multiphase Flow* **21,** 107–117.

Nishikawa, K., Sekoguchi, K. and Fukano, T. (1969) On the pulsation phenomena in gas–liquid two-phase flow. *Bull. JSME* **12,** 1410–1416.

Olszowksi, S. T., Coulthard, J. and Sayles, R. S. (1976) Measurement of dispersed two-phase gas–liquid flow by cross-correlation of modulated ultrasonic signals. *Int. J. Multiphase Flow* **2,** 537–548.

Ong, K. H. (1975) Hydraulic flow measurement using ultrasonic transducers and correlation techniques. Ph.D. Thesis, University of Bradford.

Peebles, F N. and Garber, H. S. (1953) Chem. Eng. Progress Report No. 49/88.

Samways, A. L. (1992) Pressure fluctuations in two-phase flows. Ph.D Thesis, University of Plymouth.

Serizawa, A., Kataoka, I. and Michiyoshi, I. (1975) Turbulence structure of air–water bubbly flow, parts I–III. *Int. J. Multiphase Flow* **2,** 221–259.

Souhar, M. (1989) Some turbulence quantities and energy spectra in the wall region in bubbly flows. *Phys. Fluids A* **1,** 1558–1565.

Tutu, N. K. (1982) Pressure fluctuations and flow pattern recognition in vertical two-phase gas–liquid flows. *Int. J. Multiphase Flow* **8,** 443–447.

Wang, S. K., Lee, S. J., Jones, O. C. and Lahey, R. T. (1987) 3-D turbulent structure and phase distribution measurements in bubbly two-phase flow. *Int. J. Multiphase Flow* **13,** 327–343.

Ward-Smith, A. J. (1980) *Internal Fluid Flow*: *The Fluid Dynamics of Flow in Pipes and Ducts*, Oxford University Press, Oxford.

Whitehead, L. G., Win, L. Y. and Waters, M. H. L. (1951) Contracting ducts of finite length. *Aeronaut Quart.* **2,** 254–271.

Xu, L. A. (1986) A pulsed ultrasound cross-correlation system for velocity measurement in two-component fluids. Ph.D. Thesis, University of Manchester.